

# Material structure generation of concrete and its further usage in numerical simulations

Martin Hušek\* and Jiří Kala<sup>a</sup>

*Institute of Structural Mechanics, Faculty of Civil Engineering, Brno University of Technology, Veveří 331/95, 602 00 Brno, Czech Republic*

*(Received November 13, 2017, Revised September 16, 2018, Accepted September 17, 2018)*

**Abstract.** The execution of an experiment is a complex affair. It includes the preparation of test specimens, the measurement process itself and also the evaluation of the experiment as such. Financial requirements can differ significantly. In contrast, the cost of numerical simulations can be negligible, but what is the credibility of a simulated experiment? Discussions frequently arise concerning the methodology used in simulations, and particularly over the geometric model used. Simplification, rounding or the complete omission of details are frequent reasons for differences that occur between simulation results and the results of executed experiments. However, the creation of a very complex geometry, perhaps all the way down to the resolution of the very structure of the material, can be complicated. The subject of the article is therefore a means of creating the material structure of concrete contained in a test specimen. Because a complex approach is taken right from the very start of the numerical simulation, maximum agreement with experimental results can be achieved. With regard to the automation of the process described, countless material structures can be generated and randomly produced samples simulated in this way. Subsequently, a certain degree of randomness can be observed in the results obtained, e.g., the shape of the failure – just as is the case with experiments. The first part of the article presents a description of a complex approach to the creation of a geometry representing real concrete test specimens. The second part presents a practical application in which the numerical simulation of the compressive testing of concrete is executed using the generated geometry.

**Keywords:** heterogeneity; material structure; noise; pressure test; smoothed particle hydrodynamics

## 1. Introduction

The complexity of computational models is constantly increasing. This phenomenon is not tied to certain fields of study-efforts to bring numerical simulations as close to reality as possible are visible everywhere, and civil engineering is no exception. When analyzing structures, the material model, the geometry and the boundary (and if needed, initial) conditions are all of importance. To a certain degree, the material model is related to the geometry or the scale at which the geometry is monitored. Why? The modeling of a heterogeneous material, e.g., concrete (a combination of aggregate, cement binder and possibly air voids) can be approached in two ways (the use of complex numerical methods will be discussed further). The first of these is to use a complex material model which expresses the behavior of concrete as a whole within a numerical simulation. Geometrically, there would be no distinction between the aggregate grains and the cement binder. In other words, heterogeneous concrete would be actually treated as a homogeneous material. The second approach is to consider concrete as it really is, i.e., made up of a mix of components. In this case a different material model would

be used for the aggregate and cement binder – probably a simpler one. However, this would require the geometric creation of a model that distinguishes between aggregate and cement binder, which could be a demanding task.

In cases when a simple geometry is used with a complex material model that replicates the heterogeneity of the mixture, various optimization, sensitivity and reliability analyses often need to be carried out (Kala 2016, Rahmanian *et al.* 2014, Miyamoto and Isoda 2012). There is a simple reason for this—a complex material model has many inputs which need to be defined. If one chooses to use a complex geometry and relatively simple material models, this problem is avoided. However, the creation of the geometry might be difficult. The complexity of boundary and initial conditions is a chapter in itself (Han *et al.* 2017, Kralik *et al.* 2015, Agrawal and Hora 2012). Again, one can imagine a situation in which the choice of geometry complexity has a decisive impact on the difficulty of solving a numerical simulation and the procedure needed to do that—e.g., an investigation into the fire resistance of a concrete structure (Kralik *et al.* 2015). In the vast majority of cases, the basic parameters of the material are available; for instance the thermal expansion or heat capacity of aggregate. However, if it is necessary to determine the thermal characteristics of a mixture, laboratory measurements have to be taken, which is not only a costly but also a time-consuming matter. However, if separate geometries are used for the aggregate and the cement binder, these problems are eliminated completely. It is only necessary to assign each part the aforementioned material

---

\*Corresponding author, Ph.D. Student  
E-mail: [husek.m@fce.vutbr.cz](mailto:husek.m@fce.vutbr.cz)

<sup>a</sup>Associate Professor  
E-mail: [kala.j@fce.vutbr.cz](mailto:kala.j@fce.vutbr.cz)

parameters, which are available in every physics textbook.

The article is divided into two parts in such a way that readers can obtain a better overview of the presented process (first and second part of the algorithm). The first part of the article deals with the process of creating the geometry of a heterogeneous material-concrete. The selected scale is of a resolution at which the aggregate and cement binder are distinguishable. The whole process is presented as an algorithm which generates geometry from an input photo of real material. As previously mentioned, the use of this approach is motivated by the growing number of inputs demanded by material models of concrete, particularly with regard to high-speed loading (Kala and Husek 2016a, b). For example, when the Smoothed Particle Hydrodynamics (SPH) method is used for the calculation, the problem is not the discretization of the investigated domain (i.e., the complexity of the geometry) (Husek *et al.* 2016), but rather the difficulty in entering the inputs if complex computational tools are used (Nam *et al.* 2016).

Subsequently, in the second part of the article, the generated geometry of concrete-aggregate and cement binder is utilized in the simulation of a cylindrical pressure test using the SPH method. The algorithm in this part shows how the heterogeneity of the material can be enhanced by simply causing the masses of the individual SPH particles to oscillate. There are several options for the use of this numerical heterogeneity. The article shows an application of the oscillation of the masses of SPH particles within the *transition layer*-a layer where aggregate and cement binder are in contact. The conclusion of the article then summarizes the findings and the results of numerical simulations.

## 2. Possible approaches in simulations involving material heterogeneity

Numerical simulations in the area of structural mechanics involve several steps. Aside from certain special exceptions (purely analytical cases), there will always be three steps. The first of these is the creation of the simulated geometry and its discretization-this is often related to the numerical method used. The second step is the allocation of input data or values to the model created-material models and their parameters, initial and boundary conditions, or other constraints. The third step is the launch of the calculation itself, and its subsequent evaluation. In the case of complex analyses such as the analysis of the development of cracks in concrete, it is mainly the first two steps that will govern the course of the execution of the numerical simulation. In this way, three approaches can be distinguished in cases when material heterogeneities are taken into consideration in numerical simulations. The first approach utilizes complex methods, or extensions of basic numerical methods. The second employs complex material models, while the third works with a complex input geometry that represents the analysed specimens.

### 2.1 Complex numerical methods

The appearance of such methods could be described as a

modern trend. New numerical methods that should be capable of generally describing an examined event (for instance the creation of discontinuity in the studied domain) are constantly emerging. For example, if the Finite Element Method (FEM) were one of the basic methods, then the Extended Finite Element Method (XFEM) could be considered as its extension (Moës *et al.* 1999). In the FEM, *shape functions* are used to provide an approximation space so that the solution can be represented by a vector. In the classical FEM, these shape functions are polynomials. In the XFEM, additional *enrichment functions* are used to approximate the solution in addition to the polynomial shape functions. These enrichment functions are chosen to have properties that the solution is known to follow. The most obvious XFEM enrichment functions are power functions introduced at the sharp corners of cracks to represent the singularities in the solution gradient (i.e., the singularity in the stress for solid mechanics problems).

However, the use of such method is still more *academic* than *practical*. In this context, other methods and approaches can be mentioned such as the Microplane model (Bazant 1984, Bazant and Ozbolt 1990), or the Discrete crack or Smearred crack approach (Willam and Carol 1995). The key property of the mentioned methods and approaches is the use of a relatively simple geometry in combination with a relatively simple material model. However, this comes at the cost of needing to employ demanding computational operations that are included directly in the source codes of the numerical methods.

### 2.2 Simple geometry, complex material model

As already mentioned in the *Introduction*, another possible approach is to use a complex material model which is capable of describing a variable loading method in combination with a relatively simple numerical method and a relatively simple geometry. The cost of using such simplifications is balanced out by the need to describe the material in a relatively complex manner. The high number of inputs which the user has to define (Kral *et al.* 2016) is related to this. The high number is not necessarily a problem, but the actual interpretation of certain input data could be. The majority of complex material models use more parameters than simply those which have a physical dimension such as stiffness in their description. With regard to this, it is often almost impossible to fill in all the input data. There is often an effort to carry out the sensitivity analysis of certain parameters of the model before the simulation itself takes place (Hokes *et al.* 2016). This means that the majority of input data can be left at their table values. However, lengthy laboratory tests will eventually occur in the majority of cases, and before the launch of the numerical simulation itself, not insubstantial financial means will have to be devoted to the identification of parameters.

### 2.3 Complex geometry, simple material model

The last approach, which is also mentioned in the *Introduction*, is the very often ignored use of basic numerical methods and simple material models with a

complex geometry. The idea is to remove computational difficulty and the necessity to define the material parameters of the model. However, it requires a different approach to be taken to the perception of the simulated specimen. The specimen cannot be regarded as a simplified geometrical form-it should be seen as a complex material structure. In the case of concrete, this would mean (for example) the creation of the geometry of the aggregate and cement binder. Each of such geometrical models (of aggregate and cement binder) will subsequently have to be discretized according to the selected numerical method and allocated a simple material model. The question is how material structure can be created as simply but as realistically as possible.

It is popular to use one the possible methods of creating the material structure of concrete in connection with the Discrete Element Method (DEM). The method is known as the Voronoi diagram (or also as Voronoi tessellation, Voronoi decomposition or Voronoi partition), see Aurenhammer (1991). The problem with this method is its excessive perfection. The grain of the aggregate makes an artificial impression due to being without defects or randomness of shape. The perfectly straight edges can be *corrected* using a noise function. This process can be understood as a combination of two mathematical functions-a straight line and a curve oscillating around it. The straight line defines the basic shape of the aggregate and then a suitably added/subtracted noise function creates the aggregate's real appearance. This technique is nothing novel-it is widely used in computer graphics. It is based on Ken Perlin's statement (Kessenich *et al.* 2017) that "*you can think of noise as seasoning for graphics*".

#### 2.4 From the practical point of view

From the practical point of view there is a choice of three approaches. However, if the word *practical* is defined as meaning *currently usable in practice*, e.g., when designing a bridge structure, only the second and third approaches remain available. If one were to stipulate a requirement for the simplest possible process for the execution of a numerical simulation without any further costs, only the third approach would remain-i.e., the use of simple numerical methods, simple material models and a complex geometry. The article will therefore describe a process by which a complex material geometry can be created for concrete and a numerical simulation of a loading test carried out at the same time.

### 3. The first part of the algorithm

If a space exists within which a coherent noise function (coherent noise is a type of smooth pseudorandom noise) is able to generate values within a defined range, this suggests that a given set of generated values could have a specific distribution that corresponds to a certain proposed source (input). If the source is a two-dimensional space with values that are either 1 or 0, a cutting plane through the aforementioned noise function space could produce a section possessing values that are identical to those of the

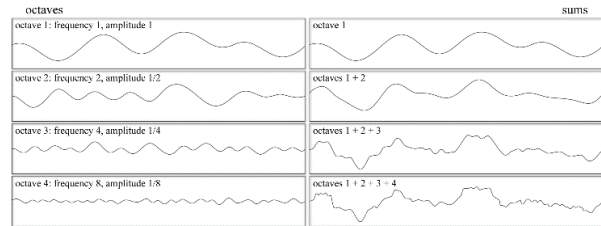


Fig. 1 Creating higher-order Perlin noise by summing the octaves of gradient-based coherent noises

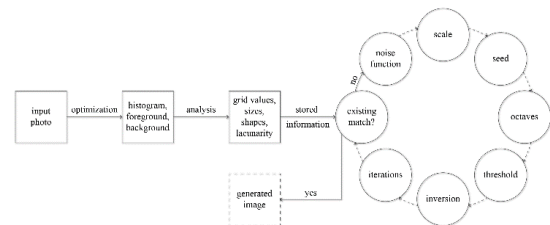


Fig. 2 Diagram of the first part of the algorithm for material structure generation based on an input photo

source for many criteria.

The coherent noise function can be arbitrary and combinable in any way with other coherent functions, for example Perlin noise (Perlin 1985). Fig. 1 shows one of the options for the creation of a higher order of coherent noise-due to its self-similar pattern it can be regarded as a fractal. Specifically, it is Perlin noise-a type of coherent noise that is the sum of several coherent-noise functions of ever-increasing frequencies and ever-decreasing amplitudes. The omission of some of the octaves can result in the creation of a very different noise. With regard to the properties that coherent noise function has:

- entering the same input value (seed) will always return the same output value,
- a small change in the input value (seed) will produce a small change in the output value,
- a large change in the input value (seed) will produce a random change in the output value, it is possible to create a pattern which corresponds to the source (input) according to the algorithm in Fig. 2.

A real photograph of material can be understood as a surface on which the values of a function can be plotted. The material is thus defined by the type of function employed, and its values. In the case of concrete, aggregate and cement binder can often be recognized in the photograph. The vast majority of photographs are in color, however, and so not suitable for the purpose of analysis. In order to be able to understand a photograph as a function (i.e., data source) with only two values, e.g., aggregate 1 and cement binder 0, the photograph must be adapted via the assignment of colors. This process is depicted in the left part of the diagram in Fig. 2. The right part of the diagram shows the construction of the noise function in such a way that the best possible agreement with the input photo is achieved.

#### 3.1 Generation of spatial geometry

To enable an easier understanding of the algorithm, the

following part of the article illustrates the process of creating the geometry of concrete with various aggregate grain shapes—the first part of the algorithm. Fig. 3 shows the aforementioned left part of the diagram from Fig. 2. The suitable adaptation of the photograph of the material allows the foreground-aggregate (black) and background-cement binder (white) to be distinguished. Black represents 1 values and white 0 values.

A series of analyses follows this adaptation, consisting in the distinguishing of shapes, sizes and the evaluation of the global value  $\Lambda$ -Lacunarity (Smith *et al.* 1996, Plotnick *et al.* 1996), based on the average values  $\lambda_{\varepsilon, g}$  determined for each size of the evaluation box with a beginning and orientation as

$$\lambda_{\varepsilon, g} = \left( CV_{\varepsilon, g} \right)^2 = \left( \frac{\sigma_{\varepsilon, g}}{\mu_{\varepsilon, g}} \right)^2 \quad (1)$$

where  $CV$  is the coefficient of variation,  $\sigma$  the standard deviation and  $\mu$  the mean, for pixels per box. There are also other Lacunarity calculation methods, e.g., those listed in Plotnick *et al.* (1993), McIntyre and Wiens (2000), Karperien (2004) or Karperien (2013). However, the values obtained do not differ from the value gained using (1). The analyzed values of the photograph of the material remain in the computer's memory and are constantly compared during noise generation. Fig. 4 shows the right part of the diagram from Fig. 2.

The generation and subsequent optimization of noise consists of several different steps. In the first step, a suitable coherent noise function is selected. Function databases are often freely accessible and, in many cases, include both original and modified noise variants (Vivo and Lowe 2015). An example is Perlin noise (Perlin 1985) with applied smoothing of transition borders, which was used in presented example and is shown in Fig. 4.

Subsequently, the scale is changed and a suitable seed value selected so that the generated image is as similar to the input photo as possible. In the next step, the algorithm tries to include the shape of the aggregate and possibly its sharpness. As the aggregate in Fig. 3 has relatively sharp edges, the number of included octaves had to be increased, see also Fig. 1. In this stage, shapes approximating those in the input photo were created in a general manner. The next optimization step consists in the use of the *threshold value*, which is related (to a certain degree) to the potential use of color inversion. The generated noise in this stage still has many colors even though it is only in grayscale. By choosing a suitable threshold value, it is possible to say which shades of gray will become black and which, in contrast, will become white—i.e., which will have the values 1 and 0. This choice can have several impacts.

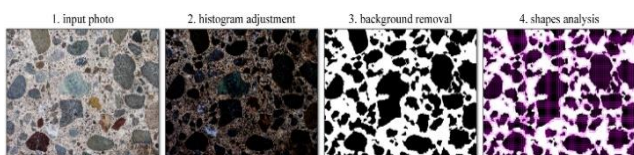


Fig. 3 Preparing the input photo for analysis

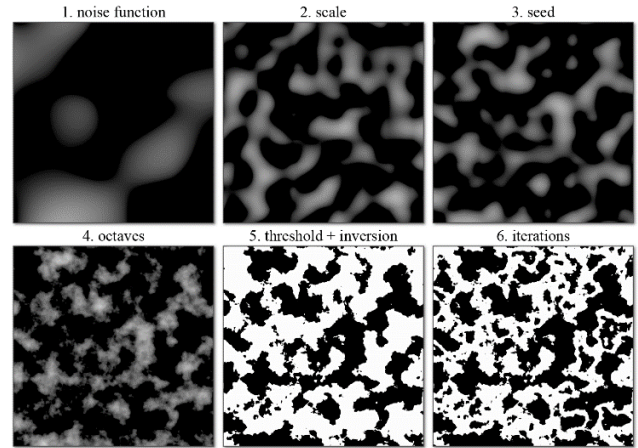


Fig. 4 Generating the structure of the material for comparison with the input photo

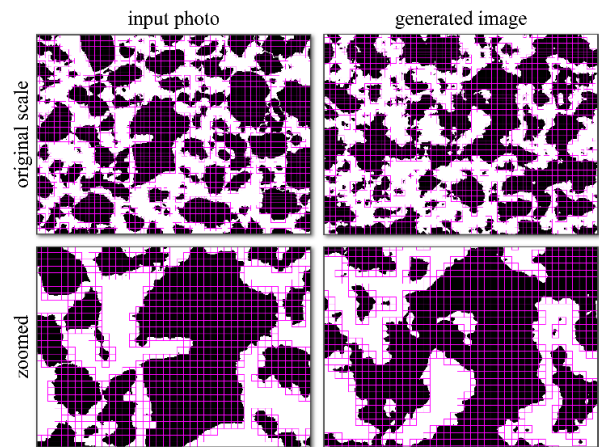


Fig. 5 Comparison of the input photo and the generated image

For example, it can, to a certain extent, alter the aggregate size which is specified by the scale value as a priority. Black and white can be inverted if one wishes to determine whether the generated noise could be improved. It should be stated that the threshold value is used for the whole time in the background of the optimization, but at a limited level. The last step of the algorithm is noise iteration. Put simply, with iterations, the noise starts to project itself onto itself and add up in a suitable manner. The obtained effect can represent additionally generated aggregate grains in places where only cement binder was present. If it is subsequently recognized that there is good congruence between the input photo and the generated image, the process of noise generation and its optimization is completed. Fig. 5 shows a more detailed comparison of the input photo and generated image.

### 3.2 Evaluation of generated geometry

As previously said, even though only a section of the material was compared, the noise functions can be seen to be spatial.

Any changes to the generated section are also projected into the noise space. Both of the generated structures,

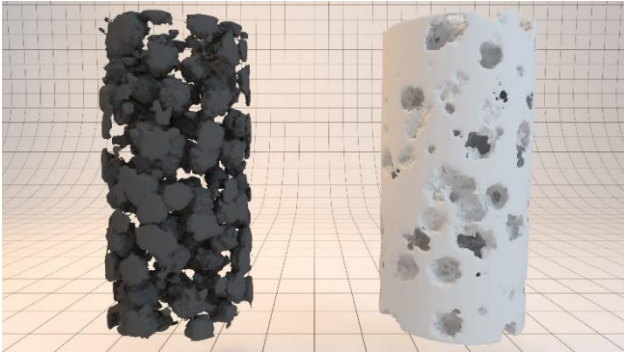


Fig. 6 Generated structure of concrete. From the left: aggregate and cement binder

aggregate and cement binder, are depicted in the form of a cylinder in Fig. 6.

As can be seen from Fig. 6, the spatial geometry of the aggregate as well as the cement binder makes a very realistic and convincing impression. The spatial arrangement of the aggregate and its size were influenced mainly by the choice of noise function, selected scale and seed value. These parameters can thus be considered to be global. The shape itself, the proportions and details of the aggregate were then influenced by the selection of the number of octaves, the threshold value level and the number of iterations. With regard to this fact, these parameters can be considered to be local. It is obvious from what was mentioned that the first part of the algorithm utilizes the descending concept of optimization, which is usual for the majority of optimization algorithms.

#### 4. The second part of the algorithm

The created aggregate and cement binder geometry can subsequently be discretized by any numerical method and then used in simulations with a suitably allocated material model. This procedure can be utilized in practically every numerical method known today, including the SPH method.

With the described process, variable results can be obtained (e.g., for cylindrical pressure tests performed on concrete) which will still correspond to those from real experiments. In this case, the *variability* concerns the failure of the concrete cylinder, and the related stress–strain curve. Thanks to this, various sensitivity analyses can be tested. There is a way to enhance the introduced heterogeneities even further, or bring them even closer to reality. It needs to be pointed out that the whole process is very simple when the SPH method is used. It is all about the use of the layer where aggregate and cement binder are in contact – the transition layer. The surface of the aggregate may not always be perfectly covered with cement binder, and the process of the solidification and hardening of cement in this area also may not be perfect. This can result in areas on the aggregate where the adhesion of the cement binder may or may not be optimal. In practice, in the case of the SPH method, this means the parameters of the particles belonging to this layer require suitable modification.

In order to continue, the spatial geometry of the



Fig. 7 Generated structure of the transition layer of concrete

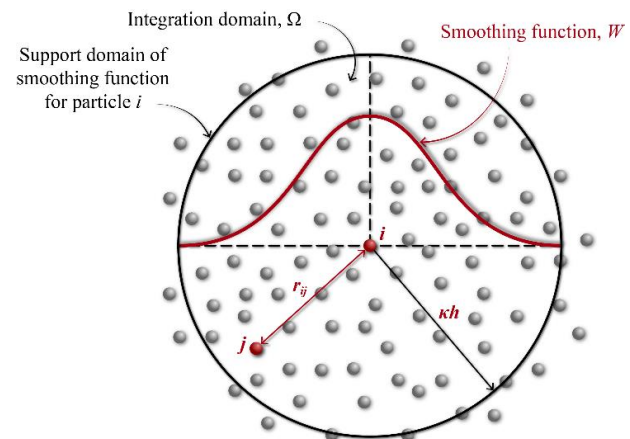


Fig. 8 Particle approximation using particles within the support domain of the smoothing function  $W$  for particle  $i$

transition layer needs to be obtained. Again, it can be obtained in several ways, e.g., by using the geometry of the aggregate or the cement binder. The contact surfaces can be considered to be the midsurface of the transition layer. The spatial geometry or volume of the transition layer can be obtained via a simple symmetrical offset in the direction of the normals of the geometry. The SPH particles which lie within the volume of the transition layer are the aforementioned particles with which the parameters will be modified. Fig. 7 shows the transition layer for the already generated aggregate and cement binder geometry.

##### 4.1 About the SPH method

The formulation of the SPH method is often divided into two key steps. The first step is the *integral representation* of field functions, and the second is *particle approximation* (Liu and Liu 2003). The concept of the integral representation of a function  $f(\mathbf{x})$  used in the SPH method starts from the following identity

$$f(\mathbf{x}) = \int_{\Omega} f(\mathbf{x}') \delta(\mathbf{x} - \mathbf{x}') d\mathbf{x}' \quad (2)$$

where  $f$  is a function of the three-dimensional position vector  $\mathbf{x}$ , and  $\delta(\mathbf{x} - \mathbf{x}')$  is the Dirac delta function given by

$$\delta(\mathbf{x} - \mathbf{x}') = \begin{cases} +\infty & \mathbf{x} = \mathbf{x}' \\ 0 & \mathbf{x} \neq \mathbf{x}' \end{cases} \quad (3)$$

In Eq. (2),  $\Omega$  is the volume of the integral that contains  $\mathbf{x}$ . Eq. (2) implies that a function can be represented in an integral form. Since the Dirac delta function is used, the integral representation in Eq. (2) is exact or rigorous as long as  $f(\mathbf{x})$  is defined and continuous in  $\Omega$  (Liu and Liu 2003). If the Delta function  $\delta(\mathbf{x} - \mathbf{x}')$  is replaced by a smoothing function  $W(\mathbf{x} - \mathbf{x}', h)$ , the integral representation of  $f(\mathbf{x})$  is given by

$$f(\mathbf{x}) \approx \int_{\Omega} f(\mathbf{x}')W(\mathbf{x} - \mathbf{x}', h)d\mathbf{x}' \quad (4)$$

where  $W$  is the so-called smoothing function and  $h$  is the smoothing length defining the influence area of the smoothing function  $W$ . Note that as long as  $W$  is not the Dirac delta function, the integral representation in Eq. (4) can only be an approximation (Liu and Liu 2003). The continuous integral representations concerning the SPH integral approximation in Eq. (4) can be converted into discretized forms of summation over all the particles in the support domain shown in Fig. 8. The corresponding discretized process of summation over the particles is commonly known as particle approximation.

If the infinitesimal volume  $d\mathbf{x}'$  in Eq. (4) at the location of particle  $j$  is replaced by the finite volume of the particle  $\Delta V_j$  that is related to the mass of the particles  $m_j$  by

$$m_j = \Delta V_j \rho_j \quad (5)$$

where  $\rho_j$  is the density of particle  $j$  ( $= 1, 2, \dots, N$ ) in which  $N$  is the number of particles within the support domain of particle  $j$ , then the continuous SPH integral representation for  $f(\mathbf{x})$  can be written in the following form of discretized particle approximation (Liu and Liu 2003) as

$$\begin{aligned} f(\mathbf{x}) &\approx \int_{\Omega} f(\mathbf{x}')W(\mathbf{x} - \mathbf{x}', h)d\mathbf{x}' \\ &\approx \sum_{j=1}^N f(\mathbf{x}_j)W(\mathbf{x} - \mathbf{x}_j, h)\Delta V_j \\ &\approx \sum_{j=1}^N f(\mathbf{x}_j)W(\mathbf{x} - \mathbf{x}_j, h)\frac{1}{\rho_j}(\rho_j \Delta V_j) \\ &\approx \sum_{j=1}^N f(\mathbf{x}_j)W(\mathbf{x} - \mathbf{x}_j, h)\frac{1}{\rho_j}(m_j) \end{aligned} \quad (6)$$

or just

$$f(\mathbf{x}_i) \approx \sum_{j=1}^N \frac{m_j}{\rho_j} f(\mathbf{x}_j)W(\mathbf{x}_i - \mathbf{x}_j, h) \quad (7)$$

Eq. (7) states that the value of a function at particle  $i$  is approximated using the average of those values of the function at all the particles in the support domain of particle  $i$  weighted by the smoothing function shown in Fig. 8.

#### 4.2 Size of the support domain

The extent of the support domain is defined according to Fig. 8 as the size of the generally variable parameter  $h$ , which is called the smoothing length. Parameter  $h$  can also be multiplied by constant  $\kappa$ . Particles which are inside the

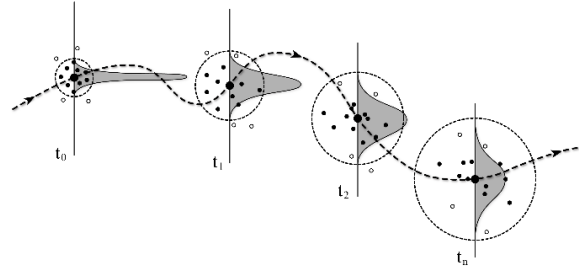


Fig. 9 Eulerian kernel-the amount of particles within the support domain might not be constant

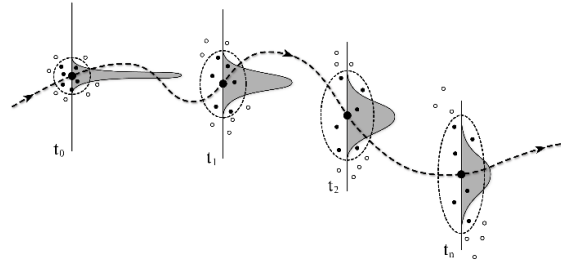


Fig. 10 Lagrangian kernel-the amount of particles within the support domain is constant

support domain attributable to particle  $i$  are called neighbouring particles. If the resultant value of the product  $\kappa h$  in each time step of the numerical simulation is the same, there can be the decrease in the number of neighbouring particles and thus also the decrease in the accuracy of the solution due the effect of excessive deformations (i.e., during the mutual divergence of the SPH particles). It is advisable to change the size of the support domain during the calculation in such a way that the number of neighbouring particles is constant.

There are many ways to dynamically develop  $h$  so that the number of neighbouring particles remains relatively constant. Benz (1989) suggested a method of developing the smoothing length. This method uses the time derivative of the smoothing function in terms of the continuity equation

$$\frac{dh}{dt} = -\frac{1}{d} \frac{h}{\rho} \frac{d\rho}{dt} = \frac{1}{d} h \nabla \cdot \mathbf{v} \quad (9)$$

where  $d$  is the number of dimensions and  $\nabla \cdot \mathbf{v}$  is the divergence of the flow. This means that the smoothing length increases when particles separate from each other and reduces when the concentration of particles is significant. It varies in order to keep the same number of particles in the neighbourhood. Eq. (8) can be discretized using SPH approximations and calculated with other differential equations in parallel (Liu and Liu 2003).

#### 4.3 Eulerian and Lagrangian Kernels

The approach in Eq. (8) is applicable when the integral representation of field functions is formulated in spatial coordinates (Eulerian kernel). With an Eulerian kernel, the smoothing length of a particle changes through the

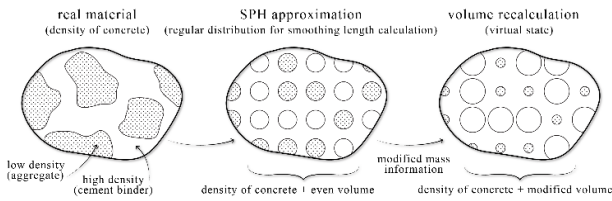


Fig. 11 Including the numerical heterogeneity into the SPH model

calculation. As a consequence, the neighbourhood of each particle needs to be updated at each time step (Husek *et al.* 2016). However, nothing exists to prevent the number of neighbouring particles changing. Despite the implementation of Eq. (8), the particles can enter and leave the support domain and thus tensile instability can occur. In other words, this means that the possibility of simulating ductile failure during the excessive divergence of particles from one another disappears. The behaviour of an Eulerian kernel during a calculation can be seen in Fig. 9.

However, when the integral representation of field functions is formulated in the material coordinates (Lagrangian kernel), the neighbours' list of each SPH particle is defined in the initial configuration and remains constant throughout the whole calculation. It means that the support domain of a particle follows material deformation in order to always keep the same neighbours. It provides a way of solving tensile instabilities (Liu and Liu 2003). The behaviour of a Lagrangian kernel during a calculation can be seen in Fig. 10.

To eliminate the tensile instabilities in the simulations the Lagrangian kernel was selected. The value of parameter  $\kappa = 1.2$  was used. In other words, the extent of the support domain was 20% bigger according to Eq. (8).

#### 4.4 SPH particles within and outside the transition layer

For an easier understanding of numerical heterogeneity and in order to avoid possible misunderstandings, a prerequisite has been introduced: all particles have the same material model allocated to them-in other words,  $\rho_j$  is the same for every  $j$  particle. At the same time, in order to eliminate the chance of the occurrence of numerical cracks (Benz 1989, Swegle *et al.* 1995, Belytschko *et al.* 2000) the particles are distributed in such a way that they are arranged into a regular grid-in other words,  $\Delta V_j$  is the same for every  $j$  particle. With regard to the above-mentioned facts, it can be concluded that every SPH particle has the same mass  $m_j$  with regard to validity Eq. (5). This state can be regarded as the initial state that exists before the creation of the material parameter oscillations themselves, and simultaneously as the next step of the second part of the algorithm. SPH particles outside the transition layer area consequently remain with their initial parameters  $\rho_j$ ,  $\Delta V_j$  and thus also  $m_j$ . SPH particles within the transition layer will have these parameters modified to a certain degree.

#### 4.5 How to amplify heterogeneity

Each SPH particle can be considered a Lagrange

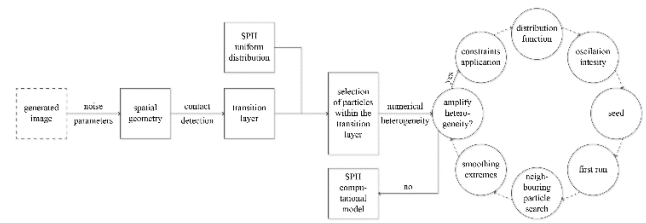


Fig. 12 Diagram of the second part of the algorithm for material structure generation based on an input photo

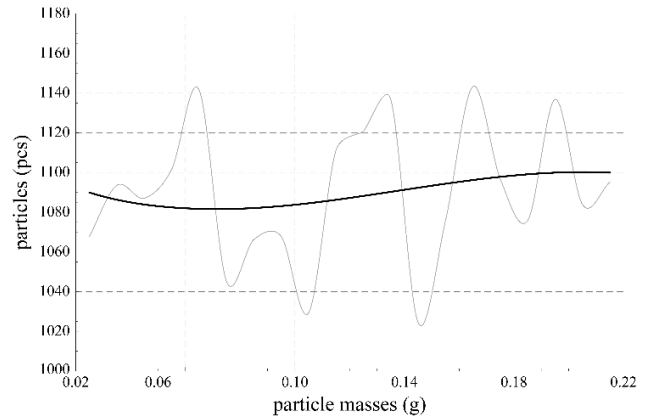


Fig. 13 One of the generated mass distribution function for particles within the transition layer

element with regard to the fact that the mass  $m_j$  allocated to a particle moves together with the particle during the simulation. Also, it can be stated that mass  $m_j$  acts in Eq. (7) as a weight coefficient. The higher the  $m_j$  value, the more particle  $j$  is going to influence its surroundings. This information can be utilized very simply to create *numerical heterogeneity* (Husek *et al.* 2017).

Numerical heterogeneity can be considered to be an adaptation of the computational model in the sense of the modification of its numerical code or of the numerical method with which the simulation is calculated. Combination is also possible. The following process can be considered a combination of both methods as it is essentially modifies the computational model as well as the numerical method. The modification consists in the introduction of the oscillation of the masses of SPH particles within the transition layer. However, this oscillation will directly precede the compilation of Eq. (7) for each  $i$  particle. In other words, the oscillation of the weight coefficient occurs directly. Other impacts may include the creation of virtual geometry in the background of the calculation as can be seen on Fig. 11; more information can be found in Husek *et al.* (2017). The process of creating numerical heterogeneity and also the rest of the second part of the algorithm can be seen in the diagram in Fig. 12.

In the first stage of the creation of numerical heterogeneity, constraints must be applied if there are any. These can be, for example, the sum of all modified masses, which has to equal the original sum of unmodified masses. In the next steps, the selection of the statistical distribution of masses and the intensity of oscillations themselves takes place. After the generation of these new masses, or weight

coefficients, the evaluation of the smoothness of the transitions of the whole generated field occurs. In other words, the sizes of the differences in oscillations between the neighboring SPH particles are evaluated. If the differences are too great, smoothing of these transitions takes place, thanks to which the simulation is more stable. If the numerical heterogeneity is then evaluated as being sufficient, the computational model is ready. Otherwise, another generated series of oscillations can be added, which further enhances the numerical heterogeneity. The distribution of masses can resemble that shown in Fig. 13, where it is depicted in the form of a histogram interleaved by a curve of a selected statistical distribution.

## 5. Numerical simulations

To illustrate the functionality of the algorithm, static load tests conducted on cylindrical concrete specimens (numerical models or models for short) using controlled displacement were simulated. Stress-strain curves were recorded at the same time. The cylindrical specimens were 300 mm high and 150 mm in diameter. As one of the conditions for the functionality of the introduced algorithm was the regularity of the initial particle distribution, the cylinders were discretized with 80 particles along the height and 40 particles along the width or depth. The particles were arranged into a regular grid field, not a radial one, and a total of 15 load tests were simulated. The first tested model did not contain any heterogeneities—in the following text, it is referred to as a homogeneous model. The remaining 14 heterogeneous models were created using the described algorithm. Fig. 14 demonstrates the homogeneous model and two generated heterogeneous models with representation of the masses.

The simulations involved 97,280 SPH particles in total and were performed via the LS-DYNA program (LSTC 2017). The Continuous Surface Cap Model (CSCM) was chosen as the material model of concrete to be used (Murray 2007, Murray *et al.* 2007), meaning that material was the same everywhere except for the transition layer where oscillations were included. The CSCM material model has been tested by the authors many times in the past and was selected mainly due to its great ability to capture even complex types of loading, see e.g., Kala and Husek (2016a, b), Husek *et al.* (2016) or Kral *et al.* (2016). Table 1 shows the parameters employed in the simulations.

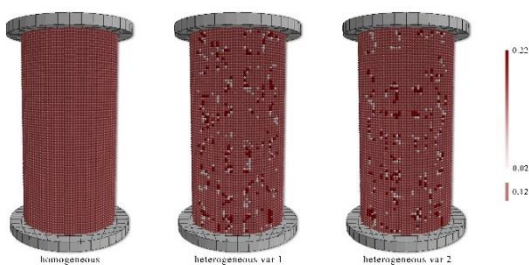


Fig. 14 From the left: Mass distribution of the homogeneous model and two generated heterogeneous models (units in g)

Table 1 The material parameters for the CSCM model

Mass density, $\rho_c$ (kgm <sup>-3</sup> )	2207
Compressive strength, $f_c$ (MPa)	47
Initial shear modulus, $G$ (GPa)	12.92
Initial bulk modulus, $K$ (GPa)	14.15
Poisson's ratio, $\nu_c$	0.18
Fracture energy, $G_F$ (Jm <sup>-2</sup> )	83.25

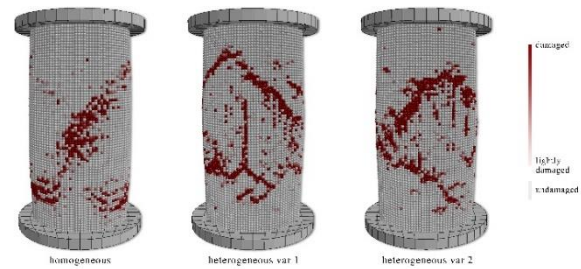


Fig. 15 From the left: Failure of the homogeneous model and two generated heterogeneous models at the end of the pressure test

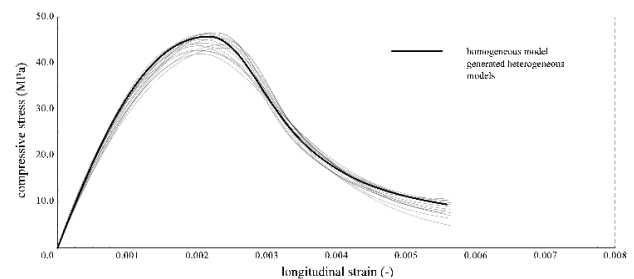


Fig. 16 Stress-strain curves of homogeneous and generated heterogeneous models

## 6. Results of the numerical simulations

The aim of the numerical simulations was the creation of variable results which still correspond to those of real experiments as much as possible. The requirement was mainly to obtain variable types of failure and the stress-strain curves which correspond to them. Thanks to the variability of the results, various sensitivity analyses can be tested, a fact which will play an important role in any possible optimization processes. As material structure from 14 different input photos supplemented with 14 unique mass oscillations was generated for the 14 tested models, there really are differences in the obtained results.

Fig. 15 shows a comparison of the failure of the homogeneous model and two generated heterogeneous models. It is obvious that the failure in each case is similar, yet different. In addition, a very standard failure with only one main crack can be observed in case of the homogeneous model since no mass oscillation was involved.

Fig. 16 shows the stress-strain curves. The homogeneous model curve is drawn with a thick line and it corresponds to results in Murray *et al.* (2007). It is clear that the heterogeneous models oscillate around this curve. However, the vast majority of the heterogeneous models do not reach the maximum load bearing capacity, i.e., 47 MPa. This can

be explained as being due to the high intensity of mass oscillations or insufficient smoothing of the oscillations of the neighboring SPH particles.

## 7. Conclusions

The first part of the article presents the process of creating spatial geometry-material structure of concrete, using an algorithm based on the comparison of an input photo of real material with the generated image of a section cut through a space filled with noise. Using a simple algorithm cycle, in which the optical congruence of the input and generated image are improved thanks to a change in the parameters of the noise functions, the spatial structure of the material is generated in the background of the process. The first part of the article presents the functionality and individual steps of the process using example of the generation of concrete with various aggregate grain shapes.

The second part of the article works with the created geometry and shows how it is possible to enhance the created heterogeneities further in the case of the use of the Smoothed Particle Hydrodynamics method. The creation of a transition layer is explained, as well as the role it plays in numerical simulations. The second part of the algorithm concentrates on the creation of numerical heterogeneity. Again, a simple cycle based on the choice of distribution function and the intensity of the oscillations of material parameters is sufficient for the creation of numerical heterogeneity. Also, numerical simulations of concrete load tests are included in the second part of the article. The functionality of the second part of the algorithm is again supported by results which demonstrate, among other things, a certain variability in the stress-strain curves of the tested numerical models.

The article as a whole presents a process which enables signs of heterogeneity to be included in numerical simulations in a very simple way.

## Acknowledgments

This outcome has been achieved with the financial support of the project GACR 17-23578S "Damage assessment identification for reinforced concrete subjected to extreme loading" provided by the Czech Science Foundation, and also with the support of the project FAST-J-17-4264 "Experimental and numerical verifications of meshfree methods in cases of dynamically loaded concrete structures" provided by the Brno University of Technology fund for specific university research.

## References

Agrawal, R. and Hora, M.S. (2012), "Nonlinear interaction behaviour of infilled frame-isolated footings-soil system subjected to seismic loading", *Struct. Eng. Mech. J.*, **44**(1), 85-107.

Aurenhammer, F. (1991), "Voronoi diagrams-a survey of a

fundamental geometric data structure", *ACM Comput. Surv.*, **23**(3), 345-405.

Bazant, Z. (1984), "Microplane model for strain-controlled inelastic behavior", *Mech. Eng. Mater.*, 45-59.

Bazant, Z. and Ozbolt, J. (1990), "Non-local microplane model for fracture, damage and size effect in structures", *J. Eng. Mech.*, **118**(11), 1119-1149.

Belytschko, T., Guo, Y., Liu, W.K. and Xiao, P. (2000), "A unified stability analysis of meshless particle methods", *Int. J. Numer. Meth. Eng.*, **48**(9), 1359-1400.

Benz, W. (1989), *Smoothed Particle Hydrodynamics: A Review*, NATO Workshop.

Han, J., Zhao, X., Tang, Z., Ma, H. and Li, Z. (2017), "Study on the bearing capacity of cold-formed steel under different boundary conditions in transmission towers", *Earthq. Struct.*, **12**(6), 665-672.

Hokes, F., Kala, J. and Krmavek, O. (2016), "Nonlinear numerical simulation of a fracture test with use of optimization for identification of material parameters", *Int. J. Mech.*, **10**, 159-166.

Husek, M., Hokes, F., Kala, J. and Kral, P. (2017), "Inclusion of Randomness into SPH Simulations", *WSEAS Trans. Heat Mass Transfer*, **12**, 1-10.

Husek, M., Kala, J., Kral, P. and Hokes, F. (2016), "Effect of the support domain size in SPH fracture simulations", *Int. J. Mech.*, **10**, 396-402.

Kala, J. and Husek, M. (2016a), "Improved element erosion function for concrete-like materials with the SPH method", *Shock Vibr.*, 1-13.

Kala, J. and Husek, M. (2016b), "High speed loading of concrete constructions with transformation of eroded mass into the SPH", *Int. J. Mech.*, **10**, 145-150.

Kala, Z. (2016), "Global sensitivity analysis in stability problems of steel frame structures", *J. Civil Eng. Manage.*, **22**(3), 417-424.

Karperien, A.B. (2004), "Defining microglial morphology: Form, function, and fractal dimension", Ph.D. Dissertation, Charles Sturt University, Sydney, Australia.

Karperien, A.B. (2013), *FracLac for ImageJ*, <<https://imagej.nih.gov/ij/plugins/fraclac/FLHelp/Introduction.htm>>.

Kessenich J., Sellers G. and Shreiner D. (2017), *OpenGL Programming Guide*, Addison-Wesley, Boston, Massachusetts, U.S.A.

Kral, P., Kala, J. and Hradil, P. (2016), "Verification of the elastoplastic behavior of nonlinear concrete material models", *Int. J. Mech.*, **10**, 175-181.

Kralik, J., Klabnik, M. and Grmanova, A. (2015), "Probability analysis of a composite steel and concrete column loaded by fire", *Appl. Mech. Mater.*, **769**, 126-132.

Liu, G.R. and Liu, M.B. (2003), *Smoothed Particle Hydrodynamics: A Meshfree Particle Method*, New Jersey: World Scientific, Hackensack, Bergen County, U.S.A.

Livermore Software Technology Corporation (2017), *LS-DYNA Theory Manual*, LSTC, Livermore, California, U.S.A.

McIntyre, N.E. and Wiens, J.A. (2000), "A novel use of the lacunarity index to discern landscape function", *Landsc. Ecol.*, **15**(4), 313-321.

Miyamoto, A. and Isoda, S. (2012), "Sensitivity analysis of mechanical behaviors for bridge damage assessment", *Struct. Eng. Mech.*, **41**(4), 539-558.

Moës, N., Dolbow, J. and Belytschko, T. (1999), "A finite element method for crack growth without remeshing", *Int. J. Numer. Meth. Eng.*, **46**(1), 131-150.

Murray, Y.D. (2007), *User's Manual for LS-DYNA Concrete Material Model 159*, FHWA-HRT-05-062.

Murray, Y.D., Abu-Odeh, A. and Bligh, R. (2007), *Evaluation of*

- Concrete Material Model 159*, FHWA-HRT-05-063.
- Nam, J.W., Yoon, I.S. and Yi, S.T. (2016), "Numerical evaluation of FRP composite retrofitted reinforced concrete wall subjected to blast load", *Comput. Concrete*, **17**(2), 215-225.
- Perlin, K. (1985), "An image synthesizer", *ACM SIGGRAPH Comput. Graph.*, **19**(3), 287-296.
- Plotnick, R.E., Gardner, R.H. and O'Neill, R.V. (1993), "Lacunarity indices as measures of landscape texture", *Landscape Ecol.*, **8**(3), 201-211.
- Plotnick, R.E., Gardner, R.H., Hargrove, W.W., Prestegard, K. and Perlmutter, M. (1996), "Lacunarity analysis: A general technique for the analysis of spatial patterns", *Phys. Rev. E*, **53**(5), 5461-5468.
- Rahmanian, I., Lucet, Y. and Tesfamariam, S. (2014), "Optimal design of reinforced concrete beams: A review", *Comput. Concrete*, **13**(4), 457-482.
- Smith, T.G., Lange, G.D. and Marks, W.B. (1996), "Fractal methods and results in cellular morphology-dimensions, lacunarity and multifractals", *J. Neurosci. Meth.*, **69**(2), 123-136.
- Swegle, J.W., Hicks, D.L. and Attaway, S.W. (1995), "Smoothed particle hydrodynamics stability analysis", *J. Comput. Phys.*, **116**(1), 123-134.
- Vivo, P.G. and Lowe, J. (2015), *The Book of Shaders*, <<http://www.thebookofshaders.com>>.
- Willam, K. and Carol, I. (1995), "Discrete Versus smeared crack analysis", *Proceedings of the 2nd International Association of Fracture Mechanics for Concrete and Concrete Structures*, Zurich, Switzerland.